Self-Assembly of a Poly(ethylene oxide)/Poly(propylene oxide) Block Copolymer (Pluronic P104, $(EO)_{27}(PO)_{61}(EO)_{27}$) in the Presence of Water and Xylene

Birgitta Svensson,[†] Paschalis Alexandridis,*[,†,‡] and Ulf Olsson[†]

Physical Chemistry 1, Center for Chemistry and Chemical Engineering, Lund University, P.O.B. 124, SE-221 00 Lund, Sweden, and Department of Chemical Engineering, State University of New York at Buffalo, Buffalo, New York 14260-4200

Received: April 8, 1998; In Final Form: July 2, 1998

The phase behavior and microstructure at 25 °C in mixtures of the amphiphilic block copolymer Pluronic P104 (with the formula $(EO)_{27}(PO)_{61}(EO)_{27}$, where EO is ethylene oxide and PO is propylene oxide), D_2O, and *p*-xylene are presented. A rich phase behavior with both normal ("oil-in-water") and reverse ("water-in-oil") phases is observed. Two isotropic micellar solutions (normal and reverse micellar solutions) and six lyotropic liquid crystalline phases (normal and reverse micellar cubic, normal and reverse hexagonal, reverse bicontinuous cubic, and lamellar phases) are formed. The structural length scales in the liquid crystalline phases were determined from small-angle X-ray scattering. The interfacial area per PEO block varies in the range 110−155 Å^2.

1. Introduction

Amphiphilic copolymers containing both hydrophilic and hydrophobic blocks are widely used in industrial processes. The molecular weight and the chemical nature of the copolymer can be adjusted to meet specific requirements of the different applications, such as dispersion stabilization, foaming, detergency, emulsification, and pharmaceutical formulations.[1] The experimental information and fundamental understanding of amphiphilic copolymer self-assembly have improved dramatically in recent years, but the phase behavior and the structure of the different phases formed are still less well-known.[2]

Amphiphilic block copolymers can form self-assembled aggregates when dissolved in a selective solvent.[3] One example is the copolymer studied here, a triblock copolymer with end blocks of hydrophilic poly(ethylene oxide) (PEO) and a middle block of less polar poly(propylene oxide) (PPO). (Such copolymers are commercially available under the trade name Pluronic (BASF) or Synperonic (ICI).) One solvent that is selective to the PEO block at 25 °C (the temperature used throughout this study) is water. Propylene oxide is only slightly soluble in water at 25 °C.[4] The PEO and PPO blocks therefore segregate, and micelles and various lyotropic liquid crystalline phases are formed depending on the composition.

At ambient temperatures, spherical micelles with a core of insoluble hydrophobic PPO and a corona of hydrated PEO are formed at low polyoxyalkylene block copolymer concentration in aqueous solution. The micellar structure has been studied extensively.[5−8] As the solubility of the PEO and PPO blocks decreases with increased temperature, the critical micellization concentration is very temperature dependent.[9−11] With sufficiently strong block segregation, lyotropic liquid crystalline phases are formed at higher copolymer concentrations. Micellar cubic, hexagonal, and lamellar phases have been reported in copolymer−water systems.[6,10,12] Polyoxyalkylene block copolymers exhibit even richer phase behavior when a third component is added, i.e., oil[13−16] or a second block copolymer.[17] Both "normal" (oil-in-water) and "reverse" (water-in-oil) liquid crystalline phases can be formed at the same temperature, depending on the ternary composition.

The self-assembly of PEO−PPO block copolymers in water and oil is a very good model system for self-assembly of block copolymers in selective solvents and is therefore important to study. Such self-assembly is related to the self-assembly of surfactants in solution and to the self-assembly of solvent-free block copolymers.[16] The present study is part of an ongoing investigation of the self-assembly of amphiphilic block copolymers where the relative block composition is kept constant (40 wt % PEO) and the total copolymer molecular weight is varied. The selective solvent for the PEO block is water, and the selective solvent for the PPO block is *p*-xylene. The block copolymer in this study is the one with the highest molecular weight in this series, Pluronic P104, $(EO)_{27}(PO)_{61}(EO)_{27}$ (molecular weight 5900 g/mol). The other copolymers studied are L44 ($(EO)_{10}(PO)_{23}(EO)_{10}$, molecular weight 2200 g/mol), L64 ($(EO)_{13}(PO)_{30}(EO)_{13}$, molecular weight 2900 g/mol),[13] and P84 ($(EO)_{19}(PO)_{43}(EO)_{19}$, molecular weight 4200 g/mol).[16] Depending on the copolymer molecular weight, the number of phases found is different. In this P104 system eight distinct phases have been identified: normal ("oil-in-water") micellar solution, normal micellar cubic, normal hexagonal, lamellar, reverse ("water-in-oil") bicontinuous cubic, reverse hexagonal, reverse micellar cubic, and reverse micellar solution. Inspection under polarized light and ^{2}H NMR have been used to delineate the phase boundaries, and small-angle X-ray scattering (SAXS) was used to characterize the structures.

2. Experimental Section

2.1. Materials and Sample Preparation. The poly(ethylene oxide) (PEO)/poly(propylene oxide) (PPO) copolymer with the trade name Pluronic P104 was a gift from BASF Corp., New Jersey. The molecular weight is ≈5900, the PEO content ≈40 wt %, and the density 1.05 g/mL, according to the manufacturer. The resulting composition is $(EO)_{27}(PO)_{61}(EO)_{27}$. Deuterated

* To whom correspondence should be addressed. e-mail palexand@eng.buffalo.edu.
† Lund University.
‡ State University of New York at Buffalo.

S1089-5647(98)01789-1 CCC: $15.00
Published on Web 09/10/1998

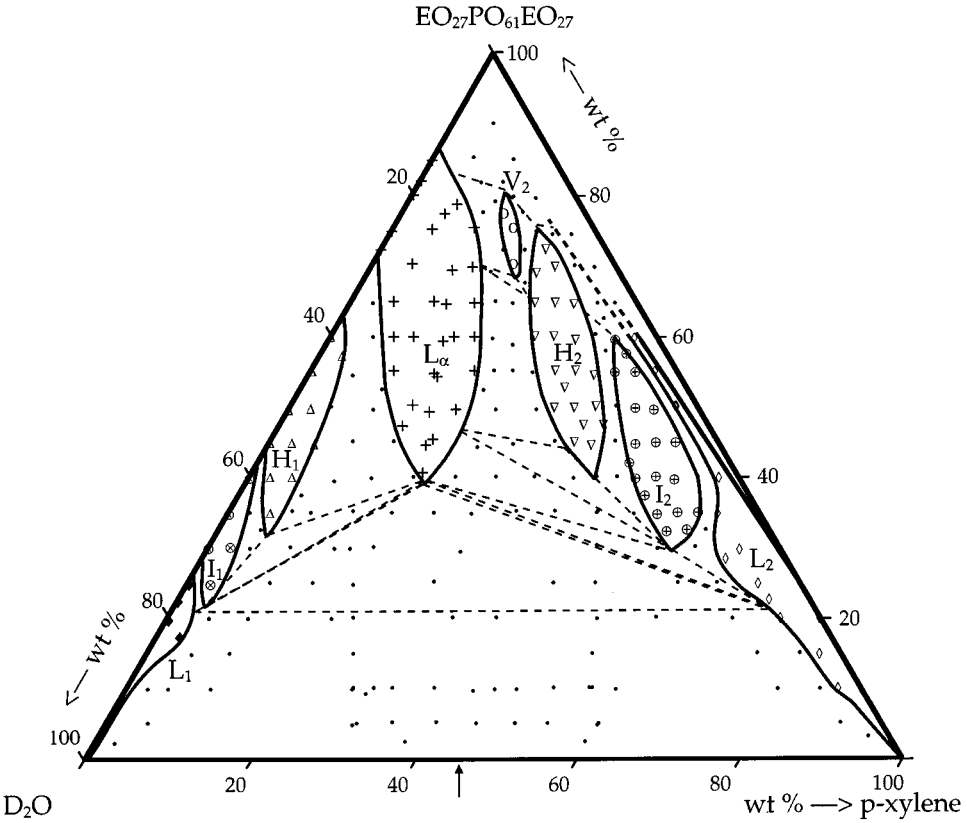

Figure 1. Phase diagram of the $(EO)_{27}(PO)_{61}(EO)_{27}/D_2O/p$-xylene system at 25 °C. The investigated samples are represented with respective symbol according to the structure: ◆, normal (water-in-oil) micellar solution (L_1); ⊗, normal micellar cubic (I_1); Δ, normal hexagonal (H_1) + lamellar (L_α); ○, reverse (water-in-oil) bicontinuous cubic (V_2); ∇, reverse hexagonal (H_2); ⊕, reverse micellar cubic (I_2); ◇, reverse micellar solution (L_2). Two- and three-phase samples are presented with the symbol ●. The arrow on the *p*-xylene axis is marking the composition where the heterogeneous samples revert from oil droplets and a water-rich L_1 phase to water droplets and an oil-rich L_2 phase. The boundaries of the various one-phase regions are indicated by solid lines, and the three-phase triangles are indicated by broken lines.

water (99.80 at. % ^2H) was purchased from Dr. Glaser AG, Basel, Switzerland. *p*-Xylene (1,4-dimethylbenzene) of purity >99.0% was obtained from Fluka Chemie AG, Buchs, Switzerland. At 25 °C the density of the deuterated water is 1.11 g/mL, and the density of *p*-xylene is 0.861 g/mL. The above stated densities were used in calculating volume fractions from weight fractions. All chemicals were used without further purification. All samples were prepared individually by weighting appropriate amounts in 8 mm i.d. glass tubes, which were flame-sealed immediately. Samples with higher copolymer concentration are very stiff. To properly mix the components, the sample tubes were centrifuged for a period of several days, repeatingly alternating the directions of the tubes. After this treatment the samples were left to stand in a 25 °C temperature-controlled room for at least 1 month.

2.2. Small-Angle X-ray Scattering (SAXS). SAXS measurements were performed on a Kratky compact small-angle system equipped with a position-sensitive detector (OED 50M from MBraun, Austria) containing 1024 channels of width 53.0 μm. Cu Kα radiation of wavelength 1.542 Å was provided by a Seifert ID-300 X-ray generator, operating at 50 kV and 40 mA. A 10 μm thick Ni filter was used to remove the Kβ radiation, and a 1.5 mm W filter was used to protect the detector from the primary beam. The sample-to-detector distance was 277 mm. To minimize the scattering from air, the camera volume was kept under vacuum during the measurements. A Peltier element controlled the temperature within 25 ± 0.1 °C. The sample holder was a 1 mm quartz capillary, and the samples were filled into the capillary by using a syringe. The obtained Bragg peaks are relatively sharp, in which case the peak position can be evaluated from the slit-smeared SAXS data.[12,13]

2.3. ^{2}H NMR. ^2H NMR experiments were performed on a Burker CXP 100 spectrometer at a resonance frequency of 15.371 MHz (magnetic field strength 2.3 T). The sample temperature was controlled by passing air of 25 ± 0.5 °C through the sample holder. NMR (often ^2H NMR on a deuterated solvent) is a convenient method for investigating phase equilibrium. In this study we applied ^2H NMR using heavy water, D_2O, as the aqueous solvent. In short, the method utilizes the fact that the spectrum from isotropic liquid and cubic phases consists of a more or less narrow singlet while hexagonal and lamellar phases give rise to quadrupolar splittings, often with significant difference in magnitude.[18] Mixtures of phases then display superpositions of the spectra from the individual phases from which the phase equilibrium can be investigated.

2.4. Delineation of the Phase Boundaries. The phase equilibrium was investigated by visual inspection of the samples in normal light and between crossed polarizers to detect optically anisotropic phases, e.g., the lamellar phase and the hexagonal phases. For higher copolymer concentrations, where centrifugation was not sufficient to produce macroscopic phase separation, phase equilibrium was also investigated by recording ^2H NMR spectra.

3. Results

3.1. Phase Diagram. The phase diagram of the $(EO)_{27}(PO)_{61}(EO)_{27}/D_2O/p$-xylene system at 25 °C is presented in Figure 1.

The boundaries of the different one-phase regions are indicated by solid lines, and approximate locations of three-phase triangles are indicated by broken lines. We note that the polyoxyalkylene block copolymer is not a pure single component but has a certain degree of polydispersity and possibly contains also other impurities. Hence, the present system is not strictly a three-component system. Three-phase regions may therefore deviate from triangles which is why they are indicated by broken lines in the phase diagram. Regions with more than three phases in equilibrium have, however, not been detected. The sample compositions investigated are indicated in the figure by different symbols depending on what one-phase or multiphase region has been observed. Heterogeneous samples belonging to two- or three-phase regions are presented as filled circles (●). The other symbols represent samples identified as belonging to homogeneous phases. The triangular phase diagram can schematically be described as an oil−water miscibility gap where the "one-phase region" at higher copolymer concentrations is decorated with a sequence of different phases. Starting from the water corner and progressing clockwise over to the oil corner, we observe the following sequence: (i) a normal (oil-in-water) micellar solution phase (denoted L_1 and with investigated sample compositions represented by the symbol ◆); (ii) a normal micellar cubic phase (I_1, ⊗); (iii) a normal hexagonal phase (H_1, Δ); (iv) a lamellar phase (L_α, +), (v) a reverse (water-in-oil) bicontinuous cubic phase (V_2, ○); (vi) a reverse hexagonal phase (H_2, ∇); (vii) a reverse micellar cubic phase (⊕, I_2); and finally (viii) a reverse micellar solution phase (◇, L_2). At lower copolymer concentrations, below the imagined miscibility gap (semicircle), we find primarily a two-phase region, $L_1 + L_2$, and a three-phase region, $L_1 + L_\alpha + L_2$.

3.2. Microstructure. In this section we present SAXS data and analyze the microstructure and length scales in the various liquid crystalline phases. To determine a quantity like interfacial area per amphiphilic molecule, we need to define explicitly the interface where this area is evaluated. To do so, we make the approximation that the system is composed of two types of components or domains, which we call polar and apolar, respectively, separated in space by sharp interfaces. The polar domains contain water and PEO blocks while the apolar domains contain the oil and the PPO blocks. With this definition, the volume fraction of the apolar domains, *f*, becomes

$$f = \phi_o + 0.62\phi_p \quad (1)$$

where ϕ_o and ϕ_p are the oil and polymer volume fractions, respectively, and 0.62 is the volume fraction of PPO in the copolymer molecule. (The PPO block, which is 60 wt % of the molecular weight, makes up ∼62 vol % of the copolymer.) In the calculations of volume fractions we have used the bulk density values of 1.05, 1.11, and 0.861 g/mL for the copolymer, D_2O, and *p*-xylene, respectively. The volume fraction of the polar domains is $1 - f$. This division of space is of course a simplification but has its significance when the SAXS diffraction patterns of the lyotropic liquid crystalline phases are analyzed. Here, as well as in previously studied systems,[13−16] this definition of the polar/apolar interface leads to interfacial areas per block copolymer molecule that varies only weakly with the composition and between different phases. This is similar to the case of nonionic surfactants.[19]

3.2.1. The Micellar Solution Phases, L_1 and L_2. The micellar solution phases, L_1 and L_2, extend from the water and oil corners, respectively. Micelle formation and micellar structure in these phases have been established in several previous studies with various polyoxyalkylene block copolymers.[2,5−10,20−25] In the L_1 phase, micelles can form without the presence of oil, while in the L_2 phase, micelle formation appears to require a

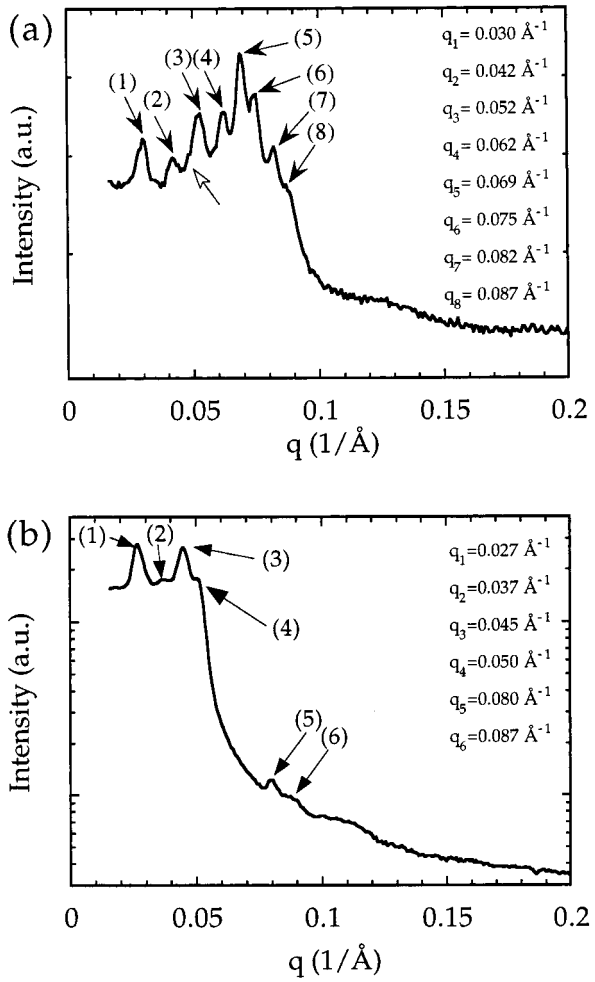

Figure 2. Slit-smeared SAXS diffraction patterns in (a) the normal micellar liquid crystalline phase, I_1, composition 31.0 vol % $(EO)_{27}(PO)_{61}(EO)_{27}$ and 69.0 vol % D_2O, (b) the reverse micellar cubic phase, I_2, composition 35.8 vol % $(EO)_{27}(PO)_{61}(EO)_{27}$, 6.7 vol % D_2O, and 57.5 vol % *p*-xylene. An unfilled arrow is used for the peak missing in the indexation to the *Pm*3*n* space group. The scattering positions of the marked peaks are given in the figures. Temperature = 25 °C.

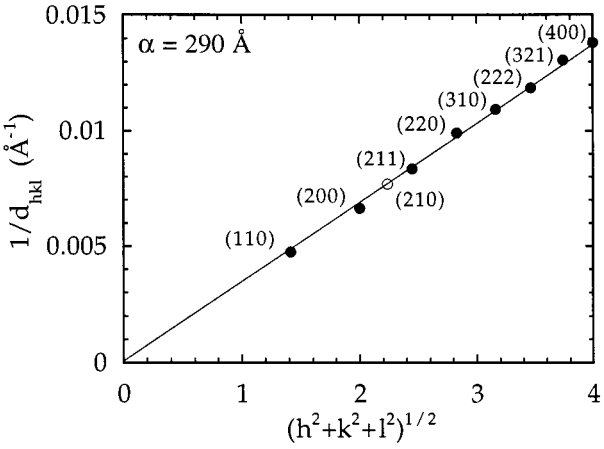

Figure 3. Plot of the reciprocal *d* spacing ($1/d_{hkl}$) of the reflections marked in the SAXS diffraction pattern of Figure 2a plotted versus $(h^2 + k^2 + l^2)^{1/2}$. An open symbol is used for the reflection (210) that was not observed in the SAXS pattern in Figure 2a.

small amount of water.[22,26−28] In this respect the polyoxyalkylene block copolymers are similar to nonionic surfactants of the alkyloligoethylene oxide type.[29] We note, however, that both the normal micelles in the L_1 phase and the reverse micelles in the L_2 phase of polyoxyalkylene block copolymer/D_2O/*p*-xylene systems are very poor solubilizers compared to low molecular weight nonionic surfactans. No more than 2.5 wt % *p*-xylene can be solubilized in the normal micelles. This is equivalent to ∼0.2 *p*-xylene molecules per PO segment. The reverse micelles can solubilize a maximum of ∼8 wt % water, equivalent to 2.1 water molecules per EO segment.

In both the water and in the oil continuous regions, we go from a micellar solution phase to a micellar cubic phase, when increasing the copolymer concentration. The micellar size is approximately constant within the copolymer concentration range of the micellar solution to the micellar cubic phase in polyoxyalkylene solution systems.[6,30] The micellar dimension and aggregation number in the L_2 phase have been investigated by several authors using scattering and fluorescence quenching techniques for polyoxyalkylene block copolymers with 40% PEO and 60% PPO and with different molecular weights.[22,26,30,31] The composition dependence of the degree of self-association has been addressed by NMR self-diffusion experiments.[32]

3.2.2. The Micellar Cubic Phases, I_1 and I_2. At higher copolymer concentrations (and at micelle volume fractions corresponding to those of hard-sphere crystallization), the micelles crystallize into a cubic lattice. The L_1-I_1 and L_2-I_2 phase transitions are easy to detect with the eye since the cubic phases are significantly more viscous. Similar to the liquid phases, the cubic phases are optically isotropic (nonbirefringent). While the small-angle X-ray scattering patterns from the liquid phases are rather featureless, with a single broad correlation peak at higher copolymer concentrations, the cubic phases display diffraction patterns with several diffraction peaks, demonstrating long-range order. In parts a and b of Figure 2 we show examples of observed diffraction patterns from the I_1 and I_2 phase, respectively. The lattice parameter, α (the cubic unit cell size), of a cubic structure is given by

$$\alpha = \frac{2\pi\sqrt{h^2 + k^2 + l^2}}{q_{hkl}} \tag{2}$$

where q_{hkl} is the scattering vector of the [*hkl*] reflection and *h*, *k*, and *l* are the Miller indices. By indexing the various reflections and plotting the reciprocal spacing ($1/d_{hkl} = q_{hkl}/2\pi$) for the reflections versus $(h^2 + k^2 + l^2)^{1/2}$, the lattice parameter is given as the inverse of the slope.

The eight marked reflections in the normal micellar cubic diffraction pattern in Figure 2 can be indexed to a bcc packing, with all the eight first reflections present (see Figure 3). However, the lattice parameter we obtain is large, α = 290 Å. The aggregation number of the micelles can be calculated from

$$N_{agg} = \phi_p \alpha^3 / n_u \upsilon_p \tag{3}$$

where ϕ_p is the copolymer volume fraction, n_u is the number of the micelles in the cubic unit cell, and υ_p is the volume of one copolymer molecule (≈9400 Å^3 for copolymer P104, obtained from the molecular weight and the density). For spherical micelles we can also calculate the interfacial area per PEO block, a_p, at the polar−apolar interface by considering the radius of the apolar core (the area per copolymer equals $2a_p$):

$$r_{sph} = 3f\upsilon_p / \phi_p 2a_p \tag{4}$$

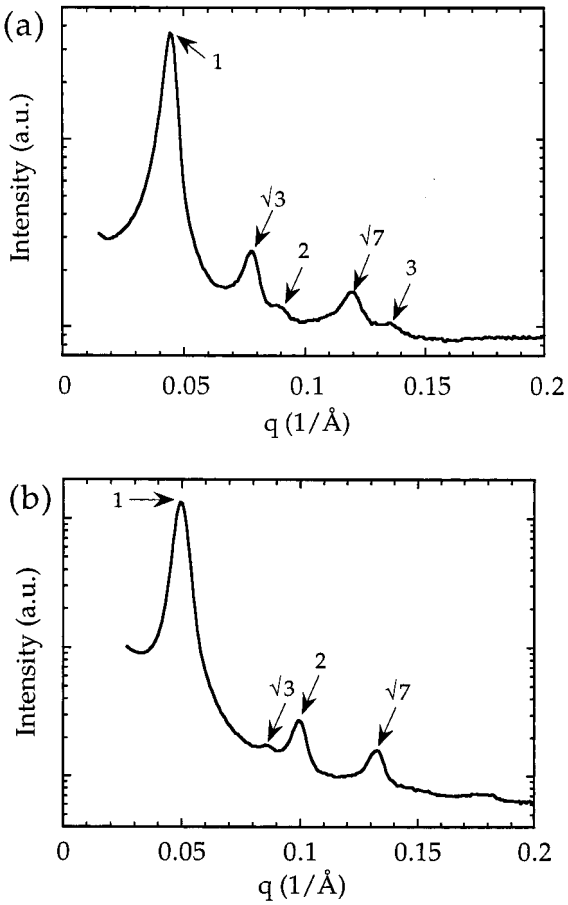

Figure 4. Representative slit-smeared SAXS diffraction pattern in (a) the normal hexagonal phase, H_1, composition 45.3 vol % $(EO)_{27}(PO)_{61}(EO)_{27}$, 48.0 vol % D_2O, and 6.7 vol % *p*-xylene, (b) the reverse hexagonal phase, H_2, composition 51.0 vol % $(EO)_{27}(PO)_{61}(EO)_{27}$, 13.3 vol % D_2O, and 35.7 vol % *p*-xylene. The Bragg peaks are marked with arrows and the relative position numbers. Temperature = 25 °C.

where the apolar volume fraction *f* obeys the relation

$$f = n_u(4\pi r_{sph}^3)/\alpha^3 \tag{5}$$

Substituting eq 5 in eq 4, we obtain

$$a_p = (36\pi n_u f^2)^{1/3}(\upsilon_p/\phi_p 2\alpha) \tag{6}$$

The values of N_{agg} and a_p obtained assuming the bcc structure ($n_u = 2$) are 402 and 106 Å^2, respectively. The value of a_p is considerably lower than the area, 154 Å^2, measured in the adjacent H_1 phase at lower copolymer concentration. Furthermore, since the general trend is that the interfacial area increases with decreasing copolymer concentration, we rather expect the interfacial area per PEO block to be larger in the I_1 phase compared to the H_1 phase. This indicates that we are dealing with a slightly more complex cubic structure than the bcc. This is in accordance with the surfactant systems where one in general finds relatively large lattice parameters of the micellar cubic phases that are not compatible with a simple bcc or fcc packing of spheres.[33] An alternative indexation of the diffraction data is to the space group *Pm*3*n* which share eight of the first nine reflections with the bcc structure. (*Pm*3*n* has the additional reflection [210].) In fact, the *Pm*3*n* is the most commonly observed micellar cubic structure in low molecular weight surfactants and lipid systems,[33−36] and it is likely that we have

TABLE 1: Characteristic Parameters in the H_1, H_2, L_α, and V_2 Phases

phase	ϕ_{P104}[a]	ϕ_{D_2O}[a]	ϕ_{oil}[a]	f[b]	$1-f$[b]	d, α[c] (Å)	r_c[d] (Å)	d_{apol}[e] (Å)	d_{pol}[f] (Å)	a_p[g] (Å^2)	$2L$[h] (Å)
H_1	0.36	0.58	0.06	0.28	0.72	174	49			153	
H_1	0.46	0.48	0.06	0.35	0.65	159	49			145	
H_1	0.46	0.54	0	0.29	0.71	134	38			154	
H_1	0.56	0.44	0	0.35	0.65	132	41			142	
H_1	0.66	0.34	0	0.41	0.59	130	44			133	
H_2	0.46	0.09	0.45	0.74	0.26	139	37			143	
H_2	0.51	0.09	0.40	0.71	0.29	133	37			140	
H_2	0.62	0.09	0.29	0.67	0.33	125	37			132	
H_2	0.42	0.13	0.45	0.71	0.29	165	46			140	
H_2	0.47	0.13	0.40	0.69	0.31	161	47			133	
H_2	0.51	0.13	0.36	0.67	0.33	147	44			137	
H_2	0.57	0.13	0.29	0.65	0.35	141	44			131	
L_α	0.47	0.35	0.18	0.47	0.53	148		70	78	136	
L_α	0.50	0.33	0.18	0.49	0.51	143		69	73	133	
L_α	0.54	0.28	0.18	0.51	0.49	133		68	65	130	
L_α	0.62	0.18	0.20	0.58	0.42	118		69	49	128	
L_α	0.73	0.27	0	0.45	0.55	110		50	60	118	
L_α	0.76	0.24	0	0.47	0.53	110		52	58	113	
L_α	0.83	0.17	0	0.52	0.48	101		52	49	111	
V_2	0.68	0.11	0.21	0.63	0.37	270				128	58
V_2	0.73	0.09	0.18	0.63	0.37	245				128	55

[a] Volume fraction copolymer, D_2O, and *p*-xylene, respectively. [b] f and $1-f$ are the apolar and the polar volume fractions, respectively. [c] d and α are the lattice parameters. [d] r_c is the hexagonal cylinder radius. [e] d_{apolar} is the apolar lamellae thickness and d_{polar} is the polar lamellae thickness. [f] a_p is the interfacial area per PEO block. [g] $2L$ is the apolar film thickness of the Gyroid minimal surface.

the same structure here. This structure contains eight micelles per unit cell which have been proposed, and for some systems convincingly shown, to be slightly elongated.[33,37,38] With $n_u = 8$, we obtain $N_{agg} = 100$. The interfacial area per PEO block depends on what axial ratio we expect for the slightly elongated micelles. If we assume them to be spherical, which is a simplification, we obtain $a_p = 168$ Å^2. This value increases with increasing axial ratio. The finding in the related surfactant systems is that the axial ratio is not significantly different from unity; values in the range 1.2−1.3 have been quoted.[33,39] An interfacial area per PEO block of ≈170 Å^2 here therefore is likely.

The scattering patterns from the I_2 phase were in general less well resolved (see Figure 2b), making an indexation more uncertain. The diffraction patterns, however, are similar to that observed in the I_1 phase, in particular in the sense that they appear to have a similarly large unit cell. We note that a recently investigated I_2 phase of a related ternary system with a diblock copolymer[15] was shown to be consistent with the *Fd*3*m* space group, but we are at present unable to confirm whether this space group also applies for the I_2 phase of the present system.

3.2.3. Normal and Reverse Hexagonal Phases, H_1 and H_2. In the hexagonal phases, denoted H_1 and H_2, samples are stiff and optically birefringent. The structure in hexagonal phases consists of long parallel cylindrical aggregates arranged on a two-dimensional hexagonal lattice in the plane perpendicular to the cylinder axis. In the H_1 phase the cylinders have an apolar interior (here oil and PPO) while in the H_2 phase the interior is polar (here water and PEO). Parts a and b of Figure 4 show typical SAXS patterns observed from the H_1 and H_2 phases, respectively. The diffraction pattern $1{:}\sqrt{3}{:}\sqrt{4}{:}\sqrt{7}$ confirms the two-dimensional hexagonal order. (Note that the reflection $\sqrt{4}$ in the SAXS pattern of the H_1 phase (Figure 4a) and the reflection $\sqrt{3}$ in the H_2 SAXS pattern (Figure 4b) are weak; we believe that this is due to a cancellation between the form factor and the structure factor, as the peak intensity is concentration-dependent.) The positions of the Bragg reflections correspond to

$$q_{hk} = \frac{4\pi\sqrt{h^2+k^2+hk}}{\alpha\sqrt{3}} \tag{7}$$

where q_{hk} is the scattering vector of the [hk] reflection with h and k being the Miller indices, and α is the lattice parameter (here nearest-neighbor distance). From the SAXS data we can calculate the cross section radius of the cylindrical aggregates assuming a sharp polar/apolar interface as defined above. For the H_1 phase the radius, r_c, of the interior apolar domain, of volume fraction f, is given by

$$r_c = \alpha[(\sqrt{3}/2\pi)f]^{1/2} \tag{8}$$

For the reverse cylinders in the H_2 phase, f should be replaced by $1-f$. We can also calculate the average area each polymer molecule occupies at the polar/apolar interface. The value of the interfacial area per PEO block is given by

$$a_p = \upsilon_p f/r_c\phi_p \tag{9}$$

where $\upsilon_p \approx 9400$ Å^3 is the volume per polymer molecule. (In eq 9, the apolar fraction of the block copolymer volume is divided by the core radius to generate the area; a prefactor 2 is canceled out by the fact that a_p is the area per PEO block, and the area per copolymer molecule is $2a_p$.) Also, here f is replaced by $1-f$ when considering the reverse cylinders of the H_2 phase. Using eqs 7−9, we have calculated α, r_c, and a_p from scattering data of the H_1 and H_2 phases, and the results are summarized in Table 1. The changes in α, a_p, and d_{cyl} ($2r_c$) with copolymer concentration are illustrated in Figure 6a,b. Some trends are presented below.

In the normal hexagonal phase the trend when no oil is added (Figure 6a, open symbols) reflects that increased PPO content (copolymer concentration) increases the core diameter of the cylinders. The PEO chains in the domain between the hydrophobic PPO and *p*-xylene cylinders become more densely packed, which is also indicated by the decrease in a_p. Changes in the diameter of the cylinders are seen when oil is added (Figure 6a, filled symbols). The d_{cyl} increases by almost 25% when 6 vol % oil is added at constant copolymer concentration ($\phi_p = 0.46$). This increase is due to the increased volume

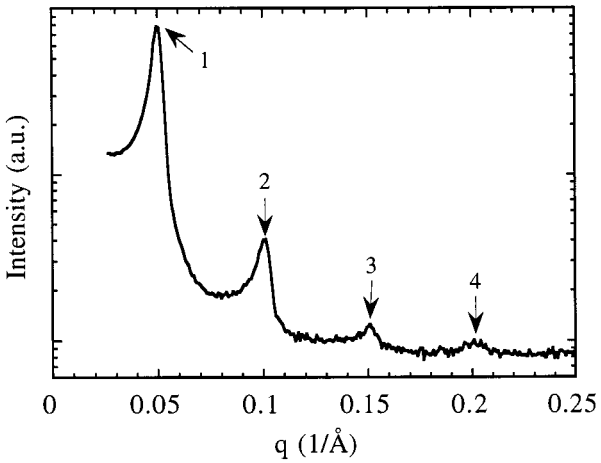

Figure 5. A representative slit-smeared SAXS diffraction pattern of the lamellar phase. The concentration is 60.0 vol % $(EO)_{27}(PO)_{61}(EO)_{27}$, 30.8 vol % D_2O, and 9.3 vol % *p*-xylene. The Bragg peaks of the first four reflections are marked with arrows and the relative position numbers. Temperature = 25 °C.

fraction of the apolar material, *f*. The variations in α and a_p indicate that the number of cylinders per unit volume decreases with addition of oil at constant copolymer content. For the reverse hexagonal phase, increased water content indicates that the number of copolymers per cylinder increases and the number of cylinders per unit volume decreases (Figure 6b, open symbols 9 vol % D_2O; filled symbols 13 vol % D_2O). Constant water content and changed copolymer concentration indicate that the packing of the PPO chains in the domain between the hydrophilic PEO and water cylinders becomes denser, and more cylinders of approximately the same size are formed per unit volume. See also refs 15 and 16 for more trends in the hexagonal phases in the polyoxyalkylene/D_2O/*p*-xylene systems.

3.2.4. The Lamellar Phase, L_α. Samples from the L_α phase are optically birefringent and less stiff compared to the samples in the H_1 and H_2 phases. The one-dimensional order gives the diffraction pattern 1:2:3:4:.... Figure 5 shows a typical diffraction pattern from the L_α phase. In general, three and occasionally four peaks were observed in the SAXS experiments. From the SAXS data we can calculate the repeat distance *d* by

$$d = 2\pi/q_1 \tag{10}$$

where q_1 is the scattering vector magnitude of the first reflection. The interfacial area per PEO block is related to *d* according to

$$a_p = v_p/\phi_p d \tag{11}$$

Within the two-domain model with sharp interfaces, we can also calculate the thickness of the polar (water plus PEO) and apolar (oil plus PPO) domains. The thickness of the apolar domain, d_{apolar}, is simply given by

$$d_{apolar} = fd \tag{12}$$

and the corresponding thickness of the polar domain is then $d_{polar} = d - d_{apolar}$. Values of *d*, a_p, d_{apolar}, and d_{polar} are given in Table 1. Some characteristic data for seven lamellar samples (concentrations are given in Table 1) are plotted versus the volume fraction of the copolymer in Figure 6c. The lamellae domain lengths vary accordingly to variations in the apolar and polar volume fractions; i.e., increased copolymer concentration leads to decreased d_{polar} distance at constant oil concentration as $1 - f$ decreases (Figure 6c, open symbols ~18 vol % *p*-xylene; filled symbols no *p*-xylene). The interfacial area per

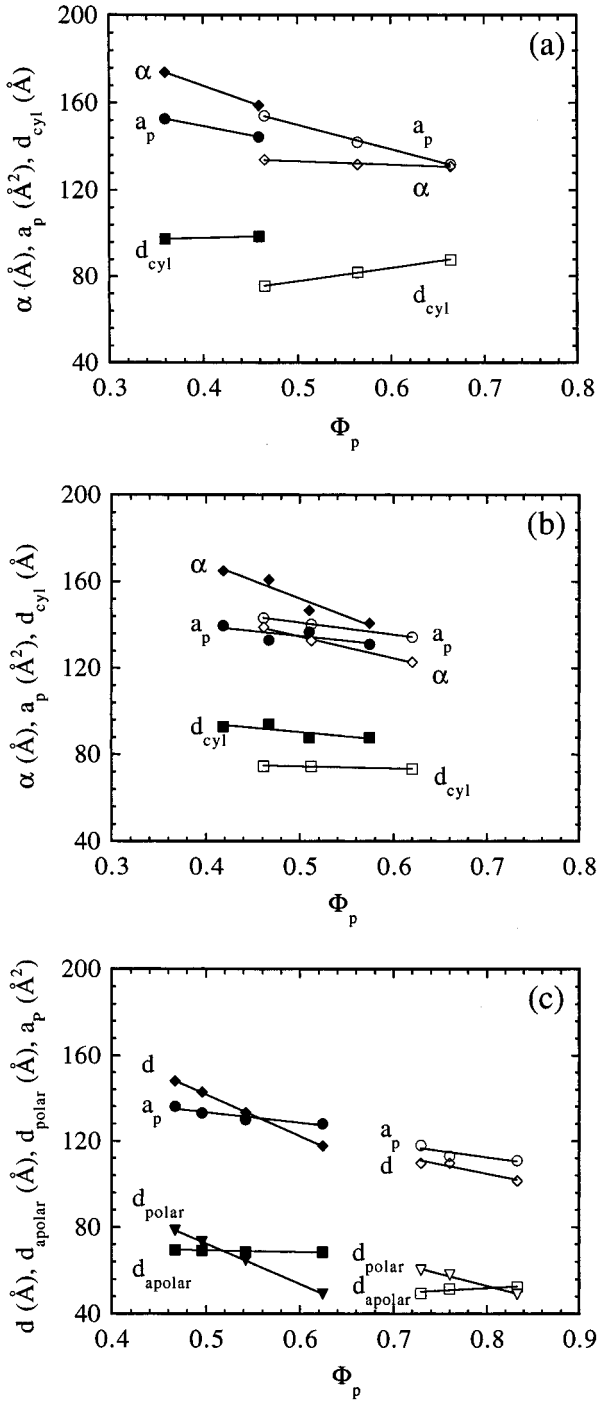

Figure 6. Characteristic structural parameters (hexagonal lattice parameter, α, lamellar lattice parameter, *d*, polar film thickness d_{polar}, apolar film thickness d_{apolar}, diameter of the apolar/polar cylinder, d_{cyl}, and interfacial area per PEO block, a_p) are plotted as a function of copolymer volume fraction, ϕ_p (data from Table 1). (a) Normal hexagonal phase. Filled symbols represent samples with varied copolymer and water concentration and constant *p*-xylene, 6.2 vol %. Unfilled symbols represent samples on the water axis where there is no *p*-xylene added. (b) Reverse hexagonal phase. Filled symbols represent samples with 13 vol % water and varied copolymer and *p*-xylene concentration. Unfilled symbols represent samples with 9 vol % water and varied copolymer and *p*-xylene concentration. (c) Lamellar phase. Filled symbols represent samples with varied copolymer and water concentration at constant volume fraction *p*-xylene (0.18−0.20), and unfilled symbols represent samples on the water axis where there is no *p*-xylene added.

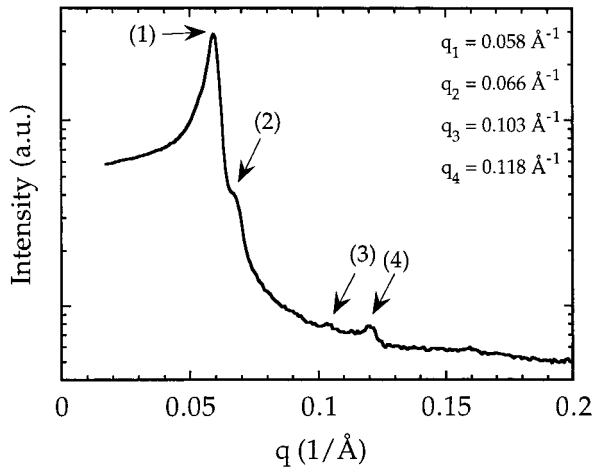

Figure 7. A representative slit-smeared SAXS diffraction pattern of the reverse bicontinuous cubic phase, V_2. The composition is 68.1 vol % $(EO)_{27}(PO)_{61}(EO)_{27}$, 11.4 vol % D_2O, and 20.5 vol % *p*-xylene. The scattering positions of the marked peaks are given in the figure. Temperature = 25 °C.

molecule decreases with increased copolymer concentration as expected (see Discussion).

3.2.5. The Bicontinuous Cubic Phase, V_2. We observe a V_2 cubic phase which is expected to have two polar labyrinths separated by an apolar film (bilayer)[36,40] in this system. The corresponding V_1 phase was not observed. Samples from the V_2 phase are stiff and optically isotropic (no birefringence). A typical SAXS pattern is shown in Figure 7. The four reflections observed can be indexed to the *Ia*3*d* space group. The first reflection corresponds to [*hkl*] = [211]. The structure of the *Ia*3*d* cubic phase is related to the Gyroid minimal surface, and this space group is by far the most commonly observed space group for bicontinuous cubic phases with surfactants and surfactant-like lipids,[34−36] and it also appears to be the most common bicontinuous cubic phase in block copolymer systems.[13,16,41,42] The size of the unit cell, the lattice parameter α, can be calculated from eq 2. Using a parallel surface construction,[40,43] we can calculate the inerfacial area per PEO block at the polar/apolar interface from the relations

$$\phi_p = \frac{\varsigma v_p}{a_p \alpha}\left(1 + \frac{2\pi\chi^u}{\varsigma}\left(\frac{L}{\alpha}\right)^2\right) \qquad (13)$$

and

$$f = \frac{2\varsigma L}{\alpha}\left(1 + \frac{2\pi\chi^u}{3\varsigma}\left(\frac{L}{\alpha}\right)^2\right) \qquad (14)$$

Here ς is a dimensionless area per unit cell, χ^u is the Euler characteristic per unit cell, and 2*L* is the apolar film thickness. For the Gyroid minimal surface $\varsigma = 3.091$ and $\chi^u = -8$.[44] The obtained values of a_p and 2*L* are presented in Table 1. The calculated a_p values (128 Å^2) are very similar to that found in the neighboring H_2 and L_α phases, thus supporting the assignment of the Gyroid structure.

3.3. Heterogeneous Regions. So far we have discussed the structure in the one-phase regions of the ternary-phase diagram. In the phase diagram (Figure 1), we have also indicated the approximate extensions of the two- and three-phase regions as determined from visual inspection, SAXS, and ^{2}H NMR experiments. The two- and three-phase regions are important for our understanding of the phase behavior as well as in applications such as emulsion stability.[45] The two major heterogeneous regions are the L_1-L_2 equilibrium at lower copolymer concentrations and the $L_1-L_\alpha-L_2$ three-phase triangle. Emulsions prepared in the L_1-L_2 two-phase region cream rather quickly. A high Ostwald ripening rate is expected since the solubility of *p*-xylene in water and vice versa is relatively high. The cream, however, is very stable (time scale of years), indicating that coalescence is a rare event. Phase inversion of the emulsions occurs at $f \approx 0.5$ (marked with an arrow on the *p*-xylene axis in Figure 1). This is consistent with the equilibrium phase diagram that is nearly symmetric with respect to the transformation $f \rightarrow 1 - f$.

4. Discussion

The phase diagram of Figure 1 differs in one important aspect from ternary-phase diagrams involving low molecular weight surfactants. Normally, the surfactant phase diagrams are less rich than the ones observed with polyoxyalkylene block copolymers. The ternary-phase diagram presented here is very rich with a total of eight different phases. The surfactants, and in particular the nonionic surfactants, can often be described as having a preferred or spontaneous mean curvature, H_0, of the polar/apolar interface, which limits the range of stable structures and reduces the richness of the phase diagram.[46] If one would apply the same concept of preferred mean curvature when discussing the polyoxyalkylene block copolymer phase diagrams, one has to allow H_0 to depend on the composition and change from a preferred curvature toward oil at high water content to a preferred curvature toward water at high oil content. This is particularly evident if we consider the $L_1 + L_\alpha + L_2$ coexistence found in the center of the phase diagram (Figure 1). Here, three different curvatures are found to coexist: the zero curvature of the lamellar phase, curvature toward oil in the L_1 phase, and curvature toward water in the L_2 phase. The corresponding three-phase region in surfactant systems occurs near zero preferred curvature and involves a so-called balanced bicontinuous microemulsion with zero mean curvature coexisting with excess oil and water phases, essentially free of surfactant.[46,47]

The area per PEO block at the polar/apolar interface, as deduced from the hexagonal (H_1 and H_2) and lamellar (L_α) phases, is in the range 110−155 Å^2. It decreases with increasing copolymer concentration as a consequence of the overlap of chains from adjacent layers. The equilibrium area per molecule, for example in the lamellar phase, results from a balance of forces. The interfacial free energy associated with the polar/apolar interface favors a small area. However, the smaller the area, the more stretched is the polymer chain, and the conformational entropy favors a larger area. In addition, we have the steric interaction between adjacent PEO "brushes" that also tend to stretch the chains. One way to quantify the degree of polymer stretching (and block segregation) is to compare the lamellar periodicity *d* with the unperturbed mean end-to-end distance. The P104 copolymer contains approximately 115 monomer units (counted as the $[CH_2CH_2O]$ sequence). A PEO homopolymer in Θ solvent having the same number of monomer units has a mean end-to-end distance of about 60 Å.[48] This is about half the lamellar repeat distance (d = 100−150 Å depending on composition; see Table 1). Another "picture" of the polymer molecules in the lamellar phase can be obtained by considering the ratio between the lamellar periodicity and the contour length of the polymer. The $(EO)_{27}(PO)_{61}(EO)_{27}$ copolymer has a contour length of approximately 400 Å. (The "length" of one EO/PO segment is ≈3.5 Å for a zigzag conformation chain.) This ratio thus varies in the range 0.25−0.4. Despite the

lamellar (smetic) ordering in the ternary system, the block copolymer itself is not highly stretched (weak segregation).

Acknowledgment. This work was supported by the Swedish Natural Science Research Council (NFR). B.S. acknowledges financial support from the Center of Competence for Amphiphilic Polymers from Renewable Resources, Lund University, Sweden. The acquisition of the SAXS apparatus was funded by the Swedish Council for Planning and Co-ordination of Research (FRN).

References and Notes

(1) Alexandridis, P. *Curr. Opin. Colloid Interface Sci.* **1996**, *1*, 490.
(2) Alexandridis, P. *Curr. Opin. Colloid Interface Sci.* **1997**, *2*, 478.
(3) Tuzar, Z.; Kratochvil, P. *Surface and Colloid Science*; Plenum Press: New York, 1993; Vol. 15.
(4) Malcolm, G. N.; Rowlingson, J. S. *Trans. Faraday Soc.* **1957**, *53*, 921.
(5) Goldmints, I.; von Gottberg, F. K.; Smith, K. A.; Hatton, T. A. *Langmuir* **1997**, *13*, 3659.
(6) Mortensen, K. *J. Phys.: Condens. Matter* **1996**, *8*, A103.
(7) Prud'homme, R. K.; Wu, G.; Schneider, D. K. *Langmuir* **1996**, *12*, 4651.
(8) Wu, G.; Chu, B.; Schneider, D. K. *J. Phys. Chem.* **1995**, *99*, 5094.
(9) Alexandridis, P.; Hatton, T. A. *Colloids Surf. A* **1995**, *96*, 1.
(10) Wanka, G.; Hoffmann, H.; Ulbricht, W. *Macromolecules* **1994**, *27*, 4145.
(11) Alexandridis, P.; Nivaggioli, T.; Hatton, T. A. *Langmuir* **1995**, *11*, 1468.
(12) Alexandridis, P.; Zhou, D.; Khan, A. *Langmuir* **1996**, *12*, 2690.
(13) Alexandridis, P.; Olsson, U.; Lindman, B. *Macromolecules* **1995**, *28*, 7700.
(14) Alexandridis, P.; Olsson, U.; Lindman, B. *J. Phys. Chem.* **1996**, *100*, 280.
(15) Alexandridis, P.; Olsson, U.; Lindman, B. *Langmuir* **1997**, *13*, 23.
(16) Alexandridis, P.; Olsson, U.; Lindman, B. *Langmuir* **1998**, *14*, 2627.
(17) Zhou, D.; Alexandridis, P.; Khan, A. *J. Colloid Interface Sci.* **1996**, *183*, 339.
(18) Khan, A.; Fontell, K.; Lindblom, G.; Lindman, B. *J. Phys. Chem.* **1982**, *86*, 4266.
(19) Rajagopalan, V.; Bagger-Jörgensen, H.; Fukuda, K.; Olsson, U.; Jönsson, B. *Langmuir* **1996**, *12*, 2939.
(20) Almgren, M.; Brown, W.; Hvidt, S. *Colloid Polym. Sci.* **1995**, *273*, 2.
(21) Brown, W.; Schillén, K.; Almgren, M.; Hvidt, S.; Bahadur, P. *J. Phys. Chem.* **1991**, *95*, 1850.
(22) Chu, B.; Wu, G. *Macromol. Symp.* **1995**, *90*, 251.
(23) Mortensen, K.; Pedersen, J. S. *Macromolecules* **1993**, *26*, 805.
(24) Wu, G.; Zhou, Z.; Chu, B. *J. Polym. Sci. Part B, Polym. Phys.* **1993**, *32*, 2035.
(25) Wu, G.; Zhou, Z.; Chu, B. *Macromolecules* **1993**, *26*, 2117.
(26) Wu, G.; Chu, B.; Schneider, D. K. *J. Phys. Chem.* **1994**, *98*, 12018.
(27) Wu, G.; Liu, L.; Buu, V.-B.; Chu, B.; Schneider, D. K. *Physica A* **1996**, *231*, 73.
(28) Zhou, S.; Su, J.; Chu, B. *J. Polym. Sci. Part B, Polym. Phys.* **1998**, *36*, 889.
(29) Olsson, U.; Jonströmer, M.; Nagai, K.; Söderman, O.; Wennerström, H.; Klose, G. *Prog. Colloid Polym. Sci.* **1988**, *76*, 75.
(30) Svensson, B.; Olsson, U.; Alexandridis, P.; Mortensen, K., to be submitted for publication.
(31) Mays, H.; Almgren, M.; Brown, W.; Alexandridis, P. *Langmuir* **1998**, *14*, 723.
(32) Barreleiro, P. A.; Andersson, K.; Håkansson, B.; Olsson, U.; Alexandridis, P., to be submitted for publication.
(33) Fontell, K.; Fox, K. K.; Hansson, E. *Mol. Cryst. Liq. Cryst. Lett.* **1985**, *1*, 9.
(34) Fontell, K. *Colloid Polym. Sci.* **1990**, *268*, 264.
(35) Mariani, P.; Luzzati, V.; Delacroix, H. *J. Mol. Biol.* **1988**, *204*, 165.
(36) Lindblom, G.; Rilfors, L. *Biochim. Biophys. Acta* **1989**, *988*, 221.
(37) Eriksson, P.-O.; Lindblom, G.; Arvidsson, G. *J. Phys. Chem.* **1985**, *89*, 1050.
(38) Johansson, L. B.-Å.; Söderman, O. *J. Phys. Chem.* **1987**, *91*, 5275.
(39) Söderman, O.; Henriksson, U. *J. Chem. Soc., Faraday Trans. 1* **1987**, *83*, 1515.
(40) Hyde, S. T. *J. Phys. Chem.* **1989**, *93*, 1458.
(41) Hajduk, D. A.; Harper, P. E.; Gruner, S. M.; Honeker, C. C.; Kim, G.; Thomas, E. L.; Fetters, L. J. *Macromolecules* **1994**, *27*, 4063.
(42) Bates, F. S.; Schultz, M. F.; Khandpur, A. K.; Förster, S.; Rosedale, J. H.; Almdal, K.; Mortensen, K. *Faraday Discuss.* **1994**, *98*, 7.
(43) Anderson, D.; Wennerström, H.; Olsson, U. *J. Phys. Chem.* **1989**, *93*, 4243.
(44) Anderson, D. M.; Davis, H. T.; Scriven, L. E.; Nitsche, J. C. C. *Adv. Chem. Phys.* **1990**, *77*, 337.
(45) Laughlin, R. G. *The Aqueous Phase Behavior of Surfactants*; Academic Press: London, 1994.
(46) Olsson, U.; Wennerström, H. *Adv. Colloid Interface Sci.* **1994**, *49*, 113.
(47) Strey, R. *Colloid Polym. Sci.* **1994**, *272*, 1005.
(48) Gregory, P.; Huglin, M. B. *Makromol. Chem.* **1987**, *187*, 1745.